

Trajectory Regularization Enhances Self-Supervised Geometric Representation

Jiayun Wang¹

Stella X. Yu^{* 1,2}

Yubei Chen^{* 3}

¹UC Berkeley

²University of Michigan, Ann Arbor

³UC Davis

peterwg@berkeley.edu, stellayu@umich.edu, ybchen@ucdavis.edu

Abstract

Self-supervised learning (SSL) has proven effective in learning high-quality representations for various downstream tasks, with a primary focus on semantic tasks. However, its application in geometric tasks remains underexplored, partially due to the absence of a standardized evaluation method for geometric representations. To address this gap, we introduce a new pose-estimation benchmark for assessing SSL geometric representations, which demands training without semantic or pose labels and achieving proficiency in both semantic and geometric downstream tasks. On this benchmark, we study enhancing SSL geometric representations without sacrificing semantic classification accuracy. We find that leveraging mid-layer representations improves pose-estimation performance by 10-20%. Further, we introduce an unsupervised trajectory-regularization loss, which improves performance by an additional 4% and improves generalization ability on out-of-distribution data. We hope the proposed benchmark and methods offer new insights and improvements in self-supervised geometric representation learning.

1. Introduction

The emergence of self-supervised learning (SSL) of image representations [2, 8, 45] has enabled many advantages over its supervised counterparts, such as discovering inherent data patterns without labels, high flexibility and generalizability when adapting to real-world data. However, most SSL is only evaluated on semantic tasks (such as classification and detection), and its effectiveness for geometric representation learning remains relatively unexplored. This is partially due to the absence of a standardized evaluation method for geometric self-supervised representations. This work establishes a new benchmark for assessing SSL’s geometric representation capabilities. We also propose methods to enhance the self-supervised geometric representation quality, including using mid-level representations and trajectory regularization.

^{*}Equal advising.

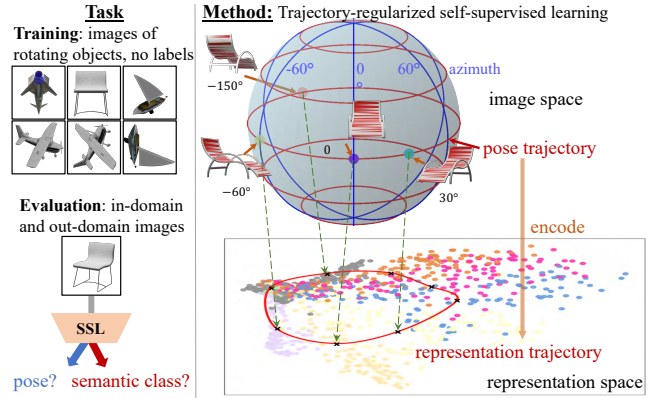


Figure 1. We study the geometric and semantic representation quality of self-supervised learning (SSL). **Left:** The model, trained exclusively on images of rotating objects, is assessed for its ability to recover the pose and semantic category of an image. **Right:** Our approach improves pose estimation accuracy by encouraging images with similar poses to form smooth trajectories in the representation space.

As mentioned earlier, the quality of SSL representations for geometric tasks is relatively underexplored, partially due to the absence of established benchmarks. This work proposes a benchmark that evaluates SSL’s performance on both semantic classification and pose estimation for object-centric images. First, we define a setting where SSL should learn both semantic and geometric representations. Our benchmark precludes the use of semantic or pose labels during training and encompasses both semantic classification and pose estimation downstream tasks during evaluation, unlike existing settings [21, 32] which allow training SSL with pose labels. Additionally, we enable out-of-domain pose estimation by introducing relative pose estimation. Without the necessity of defining category-specific canonical pose, SSL can be flexibly evaluated on out-of-domain data and unseen categories. Finally, our benchmark provides data generation configurations, leading to a dataset containing images of different objects with different poses, which is challenging for both semantic and geometric downstream tasks. Images are also sampled as short se-

Table 1. Unlike supervised learning which requires labels in training, SSL uses neither semantic nor geometric labels in training and offers improved model flexibility and generalizability. Trajectory-regularized SSL further enhances geometric representations with an unsupervised geometry-trajectory-regularization loss.

Method	semantic label	pose label	traj. reg.
Fully-Supervised [33, 48]	✓	✓	✗
Geometry-Supervised [16, 21]	✗	✓	✗
Invariant SSL (baseline) [2, 8]	✗	✗	✗
Trajectory-Regularized SSL (ours)	✗	✗	✓

quences with slight camera pose changes. The sequence could serve as a natural prior since humans and animals have access to video data instead of i.i.d. samples.

Based on the benchmark, we evaluate the geometric representation quality of existing SSL methods and discover that using mid-layer representation for pose estimation leads to 10-20% performance gain compared to the feature from the higher layers, likely owing to its similarity to patch embedding and alignment with mid-level vision tasks. Next, we propose a trajectory regularization method to encourage adjacent frames from the image sequences to form a smooth trajectory in the representation space, inspired by slow feature analysis [13, 20, 23, 44]. The trajectory regularization uses a simple local linearity assumption and leads to an additional 4% improvement for pose estimation without affecting semantic classification. Furthermore, we provide qualitative visualization and quantitative evaluation on a real-world rotating-car dataset Carvana [40] to further confirm the effectiveness of the proposed method.

To summarize, our contributions are:

- 1. Introduction of a Novel Benchmark for Geometric SSL Evaluation.** We present a new benchmark for evaluating both geometric and semantic representations of self-supervised learning, which defines the problem setting and allows evaluations on out-of-domain data.
- 2. Improving Pose Estimation with Mid-Layer Representations.** We find mid-layer representations lead to pose estimation gain (10%-20%), partially due to their ability to capture local features like patch embedding. We compress high-dimensional mid-layer representations, striking a balance between efficiency and performance.
- 3. Proposal of Unsupervised Trajectory Regularization Loss.** We introduce a novel unsupervised trajectory regularization loss that encourages the formation of a smooth trajectory in the representation space for different views of an object. It improves pose-estimation performance (4%).

2. Related Works

Self-Supervised Learning for Semantic Downstream Tasks. There are predominantly two SSL approaches:

contrastive and non-contrastive. Contrastive methods, grounded in the InfoNCE criterion [34], include [8, 11, 12, 27]. A notable variant is clustering-based contrastive learning [4, 5, 35], which shifts focus from individual samples to cluster centroids. Non-contrastive approaches [2, 3, 9, 18, 24], on the other hand, aim to align embeddings of positive pairs, similar to contrastive learning, but with strategies to prevent representational collapse.

Common to these methods is their pursuit of invariance to data augmentations, including geometric transformations. However, this invariance could potentially impede geometric representation learning. Researchers have attempted to address this by developing less invariant representations [46], predicting augmentation parameters [22, 32, 38], or applying different transformations [16]. Yet, they primarily focus on semantic tasks like semantic classification, leaving geometric tasks such as pose estimation underexplored. This work bridges the gap by also providing the benchmark for geometric downstream tasks.

Geometry-Aware Self-Supervised Learning. In the quest for geometry-aware SSL, a prevalent method is to learn equivariant representations. Past research has utilized autoencoders, including transforming autoencoders [28], Homeomorphic VAEs [19], or [43]. Recently, EquiMod [17] and SEN [36] have introduced predictors that enable reconstruction-free representation manipulation in the latent space. Another novel approach is learning equivariant representations without prior knowledge of transformation groups, as explored in [39].

Perhaps the most relevant work to us is SIE [21], where they first provide an approach and dataset to evaluate equivariant representation learning via a downstream task of rotation matrix prediction. A critical distinction is that SIE utilizes ground-truth pose labels during training, aligning more with geometry-supervised methods, whereas our approach strictly prohibits the use of any geometric or semantic labels in SSL training. We also differ from SIE in that we evaluate pose estimation performance for out-of-domain data with relative pose.

Pose Estimation. We adopt pose estimation as a specific task to evaluate geometric representations. The object pose remains ambiguous unless a canonical pose is defined. However, defining the canonical pose can be challenging as our data consists of multi-semantic-category objects, and it is hard to define a shared canonical pose for all categories due to the difficulty of aligning two classes (e.g. airplanes and boats). We thus consider two pose estimation evaluation methods. **1) Absolute pose estimation from a single image** is only well-defined if a canonical pose (or canonical coordinate system) exists. Previous work on single-view pose estimation is therefore class-specific. For a fixed set of categories, they define canonical coordinate systems class-by-class with a prior [7, 29–31] or learned features [42]. On

the contrary, we achieve class-agnostic absolute pose estimation with k nearest neighbor retrieval (k -NN): we first ask the model to find the most k similar representations and assume they are all from the same semantic category (e.g. airplanes). As the pose labels of all instances of the same semantic category follow a consistent predefined canonical coordinate system, then the predicted pose label with k -NN should also consistently follow the canonical coordinate system. **2) Relative pose estimation from a pair of images** avoids class-specific canonical coordinate system by assuming the first image defines a canonical pose, and thus predicting the relative pose of the second image compared to the first image is not ambiguous. RelPose [33, 48] describes a data-driven method for inferring the relative pose given an image pair, and we adopt their setting for our class-agnostic relative pose estimation.

3. A Benchmark for Evaluating SSL Geometric Representations

3.1. The Problem Setting

We propose a benchmark that evaluates the SSL semantic and geometric representation quality. The SSL operates without ground-truth semantic or pose labels during training, aiming to develop representations that are aware of both the semantics and geometry of the input image. Key principles for the SSL benchmark include: **1) Training Phase:** SSL is trained purely on images, without any semantic or pose labels. This ensures that all learned information is derived directly from the image itself. **2) Evaluation Phase:** SSL should learn representations that encode both semantic and geometric information. Using different representations from the model for different tasks is fine.

Given the nature of SSL, pose labels are explicitly excluded during training to align with the principle of learning without labels. One may argue that in-plane image rotations (as suggested by [16]) could offer pseudo “pose labels”, but more complex manipulations like 3D rotations are generally unfeasible. We thus strictly avoid any labels during training. In the evaluation phase, SSL must learn both semantic and geometric representations from data, since both elements and their interplay are essential for a comprehensive understanding of the data and could benefit the overall learning process. One challenge lies in estimating the pose of an out-of-domain image, as the canonical pose is not defined. We thus introduce relative pose estimation as the metric, with details as follows.

3.2. Data and Evaluation Metrics

Our benchmark provides data generation, downstream tasks and evaluation configurations, to evaluate SSL’s capacity to capture geometric and semantic information. For data generation and configuration methods, without loss of general-

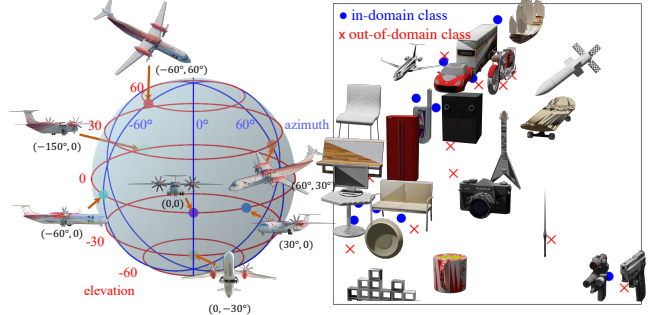


Figure 2. **Left:** We evaluate on *absolute* and *relative* pose estimation. For an object, we render images with look-at view transforms, which assume the camera is on a unit sphere with up-vector $(0, 1, 0)$ and translation $\mathbf{t} = (0, 0, 1)$. The object pose is represented as the (azimuth, elevation) of the camera angle. The figure depicts *absolute pose*, where we define a canonical pose for each category. For *relative pose*, we take two images with poses $\mathbf{p}_1, \mathbf{p}_2$ as inputs, and predict the pose difference $\Delta \mathbf{p} = \mathbf{p}_2 - \mathbf{p}_1$. **Right:** $(15^\circ, 15^\circ)$ pose of *in-domain* and *out-of-domain* semantic classes, which are plotted with PCA-projected Word2Vec [15].

izability, we use 3D meshes from ShapeNet [6] to generate images of varied objects in diverse 3D poses as the dataset used empirically in this work. For the geometric task, we adopt a fundamental one, pose estimation of object-centric images. We consider both *absolute* and *relative* 3D pose estimation tasks to enable evaluations on in-domain and out-of-domain data, where we also provide a dataset-splitting configuration. Compared to existing datasets with similar purposes [21, 49], ours enables out-of-domain evaluation and the generation method leads to a complete and even pose coverage. Shadows are also not rendered to avoid unintended ground-truth pose information leakage. We provide a detailed comparison with such datasets in supplementary.

Pose. We make source 3D objects of the same semantic class aligned and fixed for image rendering. The pose is defined as the camera pose. Specifically, we make cameras all reside on a unit S^2 sphere (Fig.2) with rendering configurations of look-at view transform with up vector $(0, 1, 0)$ and

Table 2. Number of images of in-domain and out-of-domain splits of our benchmark dataset. For semantics, we use non-overlapping 13 semantic categories as in-domain and 11 as out-of-domain data. For poses, we render distinct Fib(50) and Fib(100) for each object as in-domain and out-of-domain poses. Only 13 in-domain categories with Fib(50) poses is used for SSL training, while others are for out-of-domain evaluation. See visualizations in Fig.3.

Pose \ Semantic		in-domain	out-of-domain
		13 classes	11 classes
in-domain	Fib(50)	260k	220k
out-of-domain	Fib(100)	520k	440k

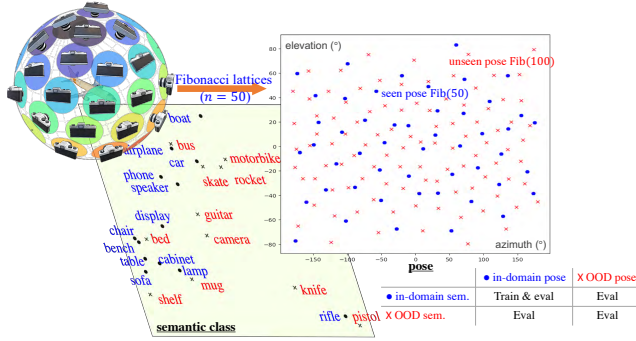


Figure 3. Our benchmark dataset includes renderings of objects from n unique camera angles, uniformly distributed across the viewing sphere S^2 , utilizing a Fibonacci sphere distribution, denoted as $\text{Fib}(n)$ (upper left shows a case where $n = 50$). We visualize the non-overlapping split of **in-domain** and **out-of-domain** semantic categories and poses. The model is trained data with both in-domain poses and semantic categories.

translation vector $(0, 0, 1)$ (following PyTorch3D’s convention [37]). Camera poses are represented as (azimuth, elevation) pairs, the spherical coordinates of camera positions. We define the category-specific canonical pose to ensure no *absolute pose* ambiguity for in-domain data as objects of each semantic category are aligned.

Relative Pose eliminates the necessity of canonical pose by considering two views of an object with pose $\mathbf{p}_1, \mathbf{p}_2$, and is defined as $\Delta \mathbf{p} = \mathbf{p}_2 - \mathbf{p}_1$, the pose difference from view 2 to view 1. Introducing relative pose ensures the SSL generalizability evaluation on out-of-domain images where canonical poses are not tractable. This differs from the previous setting [21] where out-of-domain data cannot be considered with only absolute pose estimation.

Pose Sampling. For uniform camera coverage of the whole viewing sphere, for each object, we use Fibonacci lattices [1, 25], placing n cameras at each lattice point to render n views, denoted as $\text{Fib}(n)$. We render in-domain poses using $\text{Fib}(50)$ and out-of-domain poses with $\text{Fib}(100)$, rotating $\text{Fib}(100)$ to avoid pose overlap. Fig.2 depicts rendered images with fixed pose.

Dataset Split. We divide the dataset for in-domain and out-of-domain parts (Table 2 and Fig.3 for visualizations). For the pose, we use non-overlapping $\text{Fib}(50)$ and $\text{Fib}(100)$ for in-domain and out-of-domain poses as mentioned before. For semantic categories, we use 13 object classes (e.g. airplane, car, watercraft, etc.) as in-domain data, and 11 object classes (e.g. bed, guitar, rocket, etc.) as out-of-domain data. There is no overlapping for the two sets. For each semantic category, we render 400 different objects, with 320 for unsupervised training (or probe training) and 80 for testing. For simplicity, our experiments focus on cases where either pose or semantics are out-of-domain, not both.

Downstream Tasks and Evaluation. We follow previous benchmarks for semantic classification. For geometric representation quality evaluation, our benchmark includes the

following downstream task configurations with ShapeNet [6] as an example (Fig.3): 1) *In-Domain: Absolute Pose*. Utilizing 13 in-domain semantic categories and poses from $\text{Fib}(50)$, we assess absolute pose through nearest neighbor retrieval. 2) *In-Domain: Relative Pose*. This task maintains the same data setting as the in-domain absolute pose, while the distinction lies in the training method. After unsupervised training, we employ a simple probe to train on 80% of the instances’ frozen representations for relative pose estimation, with the remaining 20% used for performance evaluation. 3) *Out-of-Domain: Unseen Poses*. We work with the 13 in-domain semantic categories but with unseen poses from $\text{Fib}(100)$. We only evaluate relative pose estimation performance with a simple probe for faster inference speed. 4) *Out-of-Domain: Unseen Semantic Categories*. This scenario involves 11 unseen semantic categories paired with in-domain poses from $\text{Fib}(50)$. Similarly, we evaluate relative pose estimation performance.

4. Enhancing Geometric Representation Learning

4.1. Mid-Layer Representation for Evaluation

We explore the feasibility of using different layers of the backbone to predict pose. This consideration stems from the understanding that geometric tasks are typically mid-level vision tasks, whereas semantic tasks align with high-level ones. Additionally, Unlike whole-image embedding which is approximately the average of local patch embeddings [14], mid-level features are local embeddings that effectively capture mid-level visual cues like pose. Mid-level features can thus be considered as a combination of patch embeddings that enhance pose estimation. We focus on whether using representations from mid-layers, such as the “conv3” or “conv4” layers (referenced in Fig.5), enhances pose estimation performance.

Empirically, our results show a significant improvement in pose estimation, with gains ranging from 10%-20% when utilizing mid-layer representations (detailed in Section 5.4). Further, as a verification of the similarity between mid-layer representations and patch embeddings, we concatenate embeddings of local image patches and observe a similar performance to “conv4” embedding (87% vs 88%, details in supplementary). However, a common challenge with mid-layer representations is their high dimensionality, primarily due to large spatial sizes. This high dimensionality can lead to inefficiencies during inference and storage. We demonstrate in Section 5.5 that these high-dimensional mid-layer representations can be effectively compressed with minimal impact on accuracy, thereby enhancing overall efficiency.

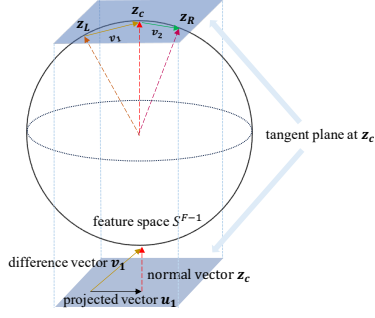


Figure 4. We enforce representations of adjacent views of an object, $\mathbf{z}_L, \mathbf{z}_C, \mathbf{z}_R$, to form a geodesic trajectory. **Upper:** \mathbf{z} resides on a unit hypersphere. The objective is to map the difference vectors $\mathbf{v}_1 = \mathbf{z}_C - \mathbf{z}_L$ and $\mathbf{v}_2 = \mathbf{z}_R - \mathbf{z}_C$ onto \mathbf{z}_C 's tangent plane, optimizing for maximal cosine similarity to achieve a linear trajectory on that plane. **Lower:** Projected vector \mathbf{u} is computed by deducting the normal component \mathbf{z}_C from the difference vector \mathbf{v} .

4.2. Trajectory Regularization

Given an image X of an object with pose \mathbf{p} , we feed it to an encoder f_θ to obtain a representation $\mathbf{z} = f_\theta(X)$, which is used for both semantic and geometric tasks.

Invariant SSL refer to methods [2, 8, 27] that generate representations that are invariant to data augmentations (e.g., random crops), which sometimes include geometric augmentations, due to the primary focus on semantic representations. For an image X , invariant SSLs create two augmented variants, X_{T_1} and X_{T_2} , which are then fed into the encoder f_θ for two respective representations, \mathbf{z}_{T_1} and \mathbf{z}_{T_2} . The invariant loss, or unsupervised semantic loss is method-dependent and can be denoted as $\mathcal{L}_{\text{sem}}(\mathbf{z}_{T_1}, \mathbf{z}_{T_2})$. Despite their focus on semantic information, we evaluate such invariant SSL representations for predicting pose $\hat{\mathbf{p}}$ of image X , considering that pose information might be encoded within \mathbf{z} .

Trajectory-Regularized SSL. We aim to enhance the SSL geometric representation quality by leveraging a natural prior: representations of objects with incremental pose changes should form a smooth, low-curvature path in the representation space. This leads us to promote a locally linear trajectory for representations corresponding to slight pose variations. Linear trajectory requires small camera pose changes only and does not violate the SSL setting.

Consider a triplet of images $\{X_L, X_C, X_R\}$ from a sequence with respective poses $\mathbf{p}_L, \mathbf{p}_C, \mathbf{p}_R$ forming a trajectory, where pose changes are small. The encoded representations $\mathbf{z}_L, \mathbf{z}_C, \mathbf{z}_R$ are normalized and residing on a unit hypersphere (i.e., $\|\mathbf{z}\|_2 = 1$). Our goal is to align these points along a geodesic trajectory on the hypersphere. This is achieved by projecting the difference vectors between representations onto the tangent plane at \mathbf{z}_C , thereby enforcing a linear trajectory as depicted in Fig.4.

The difference of two representations with adjacent poses is $\mathbf{v}_1 = \mathbf{z}_C - \mathbf{z}_L$, $\mathbf{v}_2 = \mathbf{z}_L - \mathbf{z}_C$. These vectors

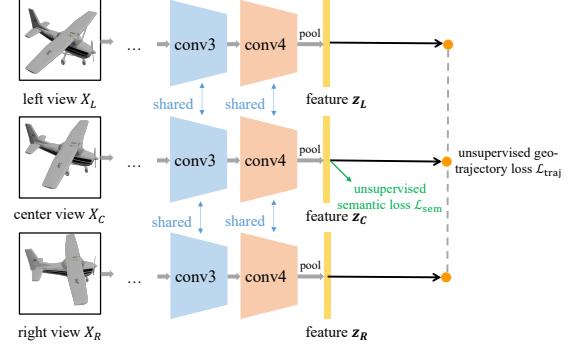


Figure 5. In addition to an unsupervised semantic loss \mathcal{L}_{sem} which is commonly used in SSL, we add a trajectory loss $\mathcal{L}_{\text{traj}}$ (Eqn.3) to enhance geometric representation. We also find mid-layer representations like “conv3” lead to pose estimation gain.

are projected on the tangent space at \mathbf{z}_C :

$$\mathbf{u}_1 = \mathbf{v}_1 - (\mathbf{v}_1 \cdot \mathbf{z}_C)\mathbf{z}_C \quad (1)$$

$$\mathbf{u}_2 = \mathbf{v}_2 - (\mathbf{v}_2 \cdot \mathbf{z}_C)\mathbf{z}_C \quad (2)$$

We then maximize the cosine similarity between \mathbf{u}_1 and \mathbf{u}_2 to enforce linearity in the trajectory. The trajectory loss, or pose loss, is defined as:

$$\mathcal{L}_{\text{traj}}(\mathbf{z}_L, \mathbf{z}_C, \mathbf{z}_R) = -\frac{\mathbf{u}_1 \cdot \mathbf{u}_2}{\|\mathbf{u}_1\| \|\mathbf{u}_2\|} \quad (3)$$

Semantic loss \mathcal{L}_{sem} is also incorporated for semantic representation capacity. We apply augmentations to X_C to generate X_{T_1} and X_{T_2} , then apply semantic loss on their representations $\mathcal{L}_{\text{sem}}(\mathbf{z}_{T_1}, \mathbf{z}_{T_2})$. Our total loss combines both semantic and pose losses (as shown in Fig.5):

$$\mathcal{L} = \mathcal{L}_{\text{sem}}(\mathbf{z}_{T_1}, \mathbf{z}_{T_2}) + \lambda \mathcal{L}_{\text{traj}}(\mathbf{z}_L, \mathbf{z}_C, \mathbf{z}_R) \quad (4)$$

where weight λ balances the trajectory loss. We always apply the trajectory loss $\mathcal{L}_{\text{traj}}$ (as per Eqn.3) at the pooled feature layer \mathbf{z} , as empirically altering the layer in $\mathcal{L}_{\text{traj}}$ impacts downstream task performance by only about 1%.

5. Experiments

5.1. Training Protocols

Our experimental framework adopts the common two-stage approach used in SSL (including supervised baselines for fair comparison). The first stage is training (or unsupervised pretraining), where the model is fed with training data. The specific training protocol is method-dependent. The second stage is evaluation, which includes directly evaluating the learned representation on downstream tasks (with the nearest neighbor) and simple probes trained on frozen representations for downstream tasks. The second evaluation stage is the same for all methods for fairness (details in Section

5.2). We mainly consider three baselines (Table 1.): fully-supervised, geometry-supervised, invariant SSL. We discuss the training settings of each method below.

Fully-Supervised Learning. We provide supervised baselines to establish an upper bound for in-domain performance (Table 3, first row). Separate models for semantic classification and pose estimation are trained with corresponding ground-truth labels to prevent task interference.

Geometry-Supervised Learning. Following methods like [16, 21, 32], we include baselines trained on ground-truth pose labels but not semantic labels during training (Table 3, second row). Specifically, we replicate the AugSelf [32] setting, combining an unsupervised semantic loss \mathcal{L}_{sem} with a cross-entropy loss for pose labels. This baseline serves as a reference and is not a direct or fair comparison to SSLs.

Invariant Self-Supervised Learning. We consider two state-of-the-art SSL methods, VICReg [2] and SimCLR [8]. Images of the same object with different poses are treated as distinct samples. We follow their training settings and use standard data augmentation (e.g. random crop and color jittering).

Trajectory-Regularized Self-Supervised Learning. We add the trajectory loss $\mathcal{L}_{\text{traj}}$ to the invariant SSL [2, 8]. As mentioned earlier, we assume image triplets from a sequence with small relative pose changes are available. We implement as follows: during training, for an image X_C with pose \mathbf{p}_C , we randomly select an adjacent left image X_L with pose \mathbf{p}_L . Using slerp [41], we obtain the right pose \mathbf{p}_R such that $\mathbf{p}_R - \mathbf{p}_C = \mathbf{p}_C - \mathbf{p}_L$, and render the right image X_R . The image triplet $\{X_L, X_C, X_R\}$ can now be used to obtain the trajectory loss. Importantly, no additional transformations like random cropping are applied to X_L, X_C, X_R to preserve geometric information. Our method still works for non-equidistant poses, i.e. $\mathbf{p}_R - \mathbf{p}_C \neq \mathbf{p}_C - \mathbf{p}_L$, with details in supplementary.

Shared Protocols. All methods utilize a ResNet-18 [26] as the backbone encoder¹. Training is consistent across models, spanning 300 epochs using the LARS optimizer [47] with a learning rate of 0.3 and weight decay of 10^{-4} .

5.2. Evaluation Protocols

Semantic Classification. We evaluate with a linear classification on top of the frozen representation from the feature layer with dimension 512.

Pose Estimation. As a comprehensive evaluation, we consider both absolute and relative pose estimation tasks: **1) Absolute pose estimation.** We employ a weighted k -nearest neighbor classifier as used in [45] on the representations from the feature layer. **2) Relative pose estimation.** We obtain feature-layer representations z_1, z_2 from two different views of an object. These representations are con-

Table 3. The proposed trajectory loss $\mathcal{L}_{\text{traj}}$ leads to pose estimation gain without harming semantic classification accuracy. Specifically, SSL achieves comparable or marginally superior results than supervised methods for out-of-domain and real data. Feature-layer representation z are used for both semantic classification and pose estimation. † We train two separate supervised models for semantic classification and pose estimation, as a single supervised multi-task model yields worse results than specialized, separate models.

Acc. (%)	in-domain		rel. pose	out-of-domain pose est.		real photos cars [40]
	sem. cls.	abs. pose		unseen pose	unseen sem.	
Fully-Sup. †	86.4	92.2	86.1	61.3	77.4	88.5
Geometry-Sup.	85.4	89.8	83.8	61.4	77.6	87.9
<i>Fully-unsupervised methods</i>						
VICReg [2]	85.6	84.3	76.7	59.6	73.1	88.7
VICReg+traj.	85.6	87.8(†3.5)	80.5(†3.8)	62.7(†3.1)	77.5(†4.4)	91.7 (†3.0)
SimCLR [8]	85.9	84.8	77.3	58.1	68.5	89.0
SimCLR+traj.	86.0	86.4(†1.6)	79.5(†2.2)	61.3(†3.2)	71.0(†2.5)	91.5(†2.5)
SimSiam [10]	85.4	84.9	77.4	57.8	68.1	88.8
SimSiam+traj.	85.5	87.2(†2.3)	79.5(†2.1)	61.0(†3.2)	70.8(†2.7)	91.2(†2.4)

catenated (resulting in a 1024-dim feature), and a simple probe of a two-layer perceptron with a hidden dimension of 1024 is used to predict the relative pose. Relative pose estimation is more computationally efficient but is generally harder as it relies on only two views for inference. We consider in-domain and out-of-domain scenarios for pose estimation and only report relative pose performance to avoid redundancy (as mentioned in Section 3.2).

5.3. Evaluation on Last Feature-Layer

We report the semantic classification and pose estimation performance of different methods in Table 3. For geometry-supervised and SSL methods, the same feature-layer representation z is used for both geometric and semantic tasks. We aim to understand: **1)** if adding trajectory loss $\mathcal{L}_{\text{traj}}$ (Eqn.3) helps pose estimation, and **2)** what is the gap between SSL and supervised methods.

Semantic Classification. All methods have a similar semantic classification accuracy (85-86%). SSL accuracies are close to the supervised upper bound. Also, adding the trajectory regularization loss $\mathcal{L}_{\text{traj}}$ leads to no accuracy loss for semantic classification, indicating that geometric representation is learned without harming semantic tasks.

In-Domain Pose Estimation. Adding the trajectory regularization yields up to 4% performance gain, although there is a performance gap between SSL methods and supervised methods. Specifically, we consider two evaluation methods: absolute pose with k -NN and relative pose with simple probe. For the absolute pose estimation, adding the proposed trajectory loss leads to 4% gain for VICReg and 2% gain for SimCLR and SimSiam. For the relative pose estimation, adding the proposed trajectory loss also leads to 4% gain for VICReg and 2% gain for SimCLR and SimSiam. For both absolute and relative pose, SSL has a 2%-3% gap to geometry-supervised methods and 4%-5% gap to the supervised methods, which is expected as SSL takes no ground-truth pose labels.

¹Our method also works with other model architecture. See supplementary for details.



Figure 6. Retrieval on a real rotating-car dataset Carvana [40]. Adding trajectory-regularization to an SSL [2] leads to better retrievals with similar pose and appearance.

Out-Of-Domain Pose Estimation. Adding trajectory loss $\mathcal{L}_{\text{traj}}$ yields up to 4% performance gain, and SSL methods are on par or even slightly outperform supervised methods on out-of-domain pose estimation. Specifically, for unseen poses, adding the proposed trajectory loss also leads to 3% gain for VICReg and 3% gain for SimCLR. SSL slightly outperforms supervised and geometry-supervised methods. For unseen categories, adding $\mathcal{L}_{\text{traj}}$ also leads to 4% gain for VICReg and 3% gain for SimCLR. SSL is on par with supervised and geometry-supervised methods.

Real Photos. Our model trained on synthetic data can directly work on real data. Specifically, we directly evaluate models trained on the synthetic dataset on a real photo dataset, Carvana [40], for pose estimation. We randomly use 80% instances as the gallery and the rest as queries. The dataset contains 318 car instances, each of which has 16 views, leading to 5,088 car images in total. Adding $\mathcal{L}_{\text{traj}}$ also leads to 3%, 3% and 2% gain for VICReg, SimCLR and SimSiam. SSL slightly outperforms supervised methods. Retrieval results are in Fig.6.

In all, adding trajectory loss enhances in-domain and out-of-domain pose estimation. SSL is on par with supervised methods on out-of-domain pose estimation.

5.4. Evaluation on Mid-Layer Representations

During training, the trajectory loss $\mathcal{L}_{\text{traj}}$ (Eqn.3) is always constrained on feature layer z , as we find changing the layer used for $\mathcal{L}_{\text{traj}}$ only gives $\sim 1\%$ difference (Section 5.7). After training the model, we could use different layers as the representation for downstream geometric tasks. We report relative pose estimation performance using representations

Table 4. Using mid-layer “conv3” rather than last-layer “feature” as representations boosts relative pose estimation accuracy: 9% for in-domain data and 20% for out-of-domain unseen poses.

Pose Acc. (%)	in-domain			unseen pose			unseen cat.		
representation layer	conv3	conv4	feat	conv3	conv4	feat	conv3	conv4	feat
Fully-Sup.	90.5	89.0	86.1	81.6	79.3	61.3	88.0	85.6	77.4
Geometry-Sup.	88.8	88.9	83.8	82.7	79.6	61.4	87.7	86.1	77.6
VICReg [2]	88.0	87.0	76.7	80.1	78.3	59.6	85.7	83.7	73.1
VICReg+traj.	89.4(↑9)	88.3	80.5	82.6(↑20)	80.3	62.7	88.2(↑11)	85.5	77.5

of different layers of ResNet-18 [26] and find mid-layer “conv3” gives the best performance (Table 4 and Fig.7). For a fair comparison, all probes have the same parameter size.

In-Domain Pose Estimation. Using mid-layer representation “conv3” greatly enhances pose estimation performance over the last feature-layer. The gap is small compared with the second to the last layer “conv4”. Specifically, using “conv3” layer as representation leads to 1% gain over “conv4” and 9% gain over “feature” layer for VICReg with trajectory regularization. For baseline SSL and supervised methods, we also observe gain with mid-level representations.

Out-Of-Domain Pose Estimation. Using the mid-layer feature “conv3” enhances pose estimation performance on out-of-domain data, and the gap is larger for unseen poses. Specifically, for unseen poses, “conv3” layer leads to 2% gain over “conv4” and 20% gain over “feature” layer for VICReg with trajectory regularization. For unseen semantic categories, “conv3” layer has 3% gain over “conv4” and 11% gain over “feature” layer. For baseline SSL and supervised methods, we also observe gain with mid-level representations for out-of-domain data.

Using Mid-Layer for Semantic Classification. Empirically, we found that using “conv3” or “conv4” layer as representation for semantic classification does not make much difference (less than 1%).

5.5. Compressing Mid-Layer Representations

Motivations and Methods. While mid-layer representations in networks like ResNet18 offer improved pose estimation accuracy, their large dimensions lead to inefficiencies. For instance, the “conv3” layer’s dimension is twice that of “conv4” and 32 times larger than the pooled “feature” layer, resulting in inefficiency due to high dimensionality. To address this, we propose compressing mid-layer representations to lower dimensions using projection heads with multi-layer perceptrons. As depicted in Fig.5, we denote the “conv3” layer representation as z^3 and the “conv4” layer representation as z^4 . We then use a projection head g_ϕ to reduce the dimensionality of these representations: for “conv3”, $y^3 = g_\phi^3(z^3)$; and similarly for

Table 5. Mid-layer representations have higher pose estimation accuracies but lower efficiency due to high dimensionality. We show they can be compressed to lower dimensions with minimal performance loss for absolute pose estimation. For relative pose estimation, compressed features have a larger gap (4-5%) but are still better than using the representation from the feature layer.

embedding	# dim	abs. pose acc. (%)	rel. pose acc. (%)
conv3	16,384	92.5	87.8
compressed conv3	512	91.4 (↓1.1)	82.4 (↓5.4)
conv4	8,192	91.9	85.2
compressed conv4	512	90.8 (↓1.1)	81.2 (↓4.0)
feature	512	87.8	77.5

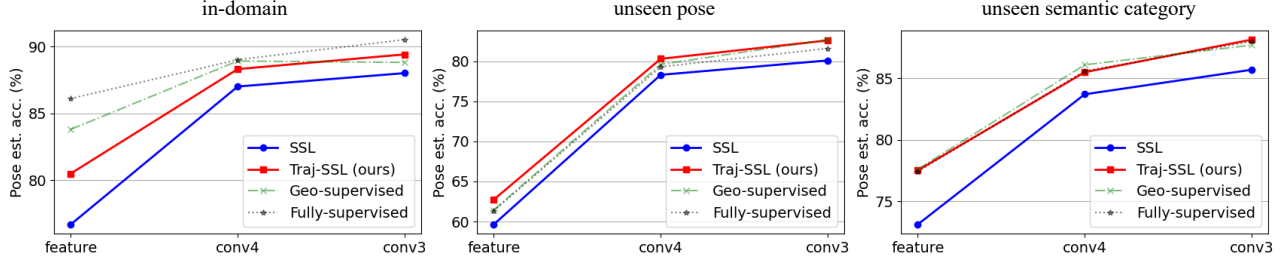


Figure 7. Mid-layer representations improve pose estimation performance: 9% for in-domain data, 20% gain for out-of-domain poses and 11% gain for out-of-domain semantic classes. SSL’s gap to supervised methods is also smaller for out-of-domain data.

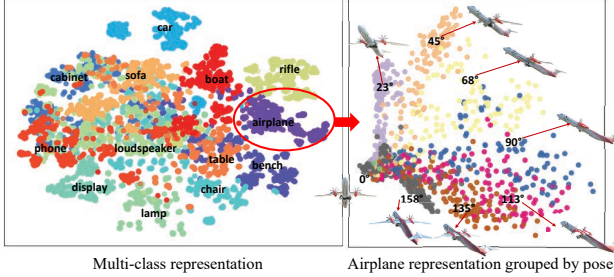


Figure 8. **Left:** We visualize representation z grouped by different semantic categories. Images with the same semantic categories form clusters. **Right:** We zoom in on one category, airplane, and visualize 200 instances with different poses. As the azimuth changes, their representation also form a trajectory.

“conv4”, $y^4 = g_\phi^4(z^4)$. More details are available in the supplementary.

Then the trajectory loss $\mathcal{L}_{\text{traj}}$ (Eqn.3) can be adapted for compressed feature y , e.g., when using “conv3” as the final representation, we can use the following trajectory loss:

$$\mathcal{L}_{\text{traj}}^{\text{conv3}}(y_L^3, y_C^3, y_R^3) = \mathcal{L}_{\text{traj}}(g_\phi^3(z_L^3), g_\phi^3(z_C^3), g_\phi^3(z_R^3)) \quad (5)$$

Results. For fair comparison, we make the compressed mid-layer representation y has dimension of 512, the same as the dimension of feature-layer z . Our findings in Table 5 demonstrate that mid-layer features can be effectively condensed 32x into smaller dimensions as “feature”-layer with only a slight reduction in performance regarding absolute pose estimation (1%). In the case of relative pose estimation, while there is a more noticeable difference in performance (4%-5%) with compressed features, they still outperform the representations derived from the feature layer.

5.6. Visualizations

Visualization of Different Semantic Categories. We present visualizations of the feature-layer z organized by different semantic categories (Fig.8). We observe that images within the same semantic categories are naturally grouped together. For a specific category, airplane, we observe that as the pose varies, the representations also cluster together, with similar poses being closer.

Visualization of Different Poses. As object poses gradually change, their representations also form a trajectory (Fig.9). We visualize the representations of 200 airplane instances with poses ranging from $(0, 30^\circ)$ to $(158^\circ, 30^\circ)$. These representations form a smooth trajectory. In contrast, the baseline method, which lacks trajectory loss, produces representations that can differentiate some views but may not form a coherent trajectory. Such representations may not perform well for pose estimation.

5.7. Hyperparameter Analysis

Our examination focuses on VICReg with proposed trajectory regularization, using relative pose estimation as the task and the feature layer for evaluation.

Layer for Trajectory Loss. In Fig.??U, we vary the layer utilized for the trajectory loss $\mathcal{L}_{\text{traj}}$ during training. Note that this is different from the setting in other experiments where trajectory loss is always constrained on feature z during training, and we change the layer as the representation for evaluation. The influence is $< 2\%$ for different layers.

Trajectory Loss Weight. In Fig.??L, the method exhibits a low sensitivity to changes in λ .

We include additional empirical studies on different backbone architectures and trajectory loss with non-equidistant poses in supplementary.

6. Summary

We introduce a new benchmark to evaluate geometric representations in self-supervised learning (SSL), where we preclude any semantic or pose label during training. Based on the evaluation of state-of-the-art SSLs on the benchmark, we identified and implemented strategies that significantly enhance geometric representation capabilities. Notably, we achieved a substantial improvement (10%-20%) in pose estimation performance by utilizing mid-layer representations. We further augmented this progress by integrating an unsupervised trajectory regularization loss, which contributes an additional 4% enhancement. The work has two limitations: **1)** Our benchmark mainly uses synthetic data. **2)** While we utilize 3D pose estimation as our primary downstream task for evaluating geometric representations,

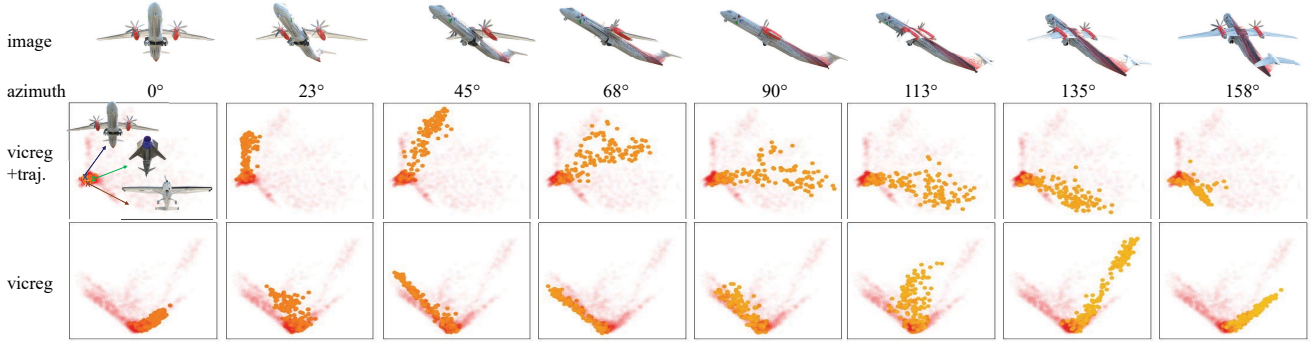


Figure 9. The visualization shows that as airplane poses change from $(0, 30^\circ)$ to $(158^\circ, 30^\circ)$, their representations form a trajectory in the feature space. While the baseline method without trajectory loss can differentiate some views, it fails to form a trajectory, which could partially contribute to worse pose estimation performance.

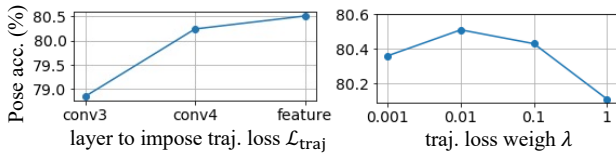


Figure 10. Hyperparameter analysis on our trajectory-regularized VICReg, which is evaluated for relative pose estimation with representation being the feature-layer z . **Left:** While fixing the feature layer for the downstream task of pose estimation, we change different layers to impose the trajectory loss \mathcal{L}_{traj} . Feature-layer gives best performance, although the difference is less than 2%. **Right:** The highest performance is achieved at trajectory loss weight $\lambda = 0.01$, though the method is not very sensitive to λ .

the inclusion of more comprehensive geometric tasks, such as 6-DoF pose estimation or depth map prediction, could enrich the benchmark’s scope and utility.

In conclusion, the proposed benchmark and approaches could augment SSL’s proficiency and offer a comprehensive understanding of semantic and geometric aspects, thereby broadening the applicability of tasks that require nuanced, generalizable and label-free learning.

Acknowledgements. The authors thank Zezhou Cheng and Quentin Garrido for helpful discussions.

References

- [1] Marc Alexa. Super-fibonacci spirals: Fast, low-discrepancy sampling of $so(3)$. In *Proceedings of the IEEE/CVF Conference on Computer Vision and Pattern Recognition*, pages 8291–8300, 2022. 4
- [2] Adrien Bardes, Jean Ponce, and Yann LeCun. Vicreg: Variance-invariance-covariance regularization for self-supervised learning. *arXiv preprint arXiv:2105.04906*, 2021. 1, 2, 5, 6, 7, 12
- [3] Adrien Bardes, Jean Ponce, and Yann LeCun. Vicregl: Self-supervised learning of local visual features. *Advances in Neural Information Processing Systems*, 35:8799–8810, 2022. 2
- [4] Mathilde Caron, Piotr Bojanowski, Armand Joulin, and Matthijs Douze. Deep clustering for unsupervised learning of visual features. In *Proceedings of the European conference on computer vision (ECCV)*, pages 132–149, 2018. 2
- [5] Mathilde Caron, Hugo Touvron, Ishan Misra, Hervé Jégou, Julien Mairal, Piotr Bojanowski, and Armand Joulin. Emerging properties in self-supervised vision transformers. In *Proceedings of the IEEE/CVF international conference on computer vision*, pages 9650–9660, 2021. 2
- [6] Angel X Chang, Thomas Funkhouser, Leonidas Guibas, Pat Hanrahan, Qixing Huang, Zimo Li, Silvio Savarese, Manolis Savva, Shuran Song, Hao Su, et al. Shapenet: An information-rich 3d model repository. *arXiv preprint arXiv:1512.03012*, 2015. 3, 4, 12
- [7] Bo Chen, Tat-Jun Chin, and Marius Klimavicius. Occlusion-robust object pose estimation with holistic representation. In *Proceedings of the IEEE/CVF Winter Conference on Applications of Computer Vision*, pages 2929–2939, 2022. 2
- [8] Ting Chen, Simon Kornblith, Mohammad Norouzi, and Geoffrey Hinton. A simple framework for contrastive learning of visual representations. In *International conference on machine learning*, pages 1597–1607. PMLR, 2020. 1, 2, 5, 6, 12
- [9] Xinlei Chen and Kaiming He. Exploring simple siamese representation learning. In *Proceedings of the IEEE/CVF conference on computer vision and pattern recognition*, pages 15750–15758, 2021. 2
- [10] Xinlei Chen and Kaiming He. Exploring simple siamese representation learning. In *Proceedings of the IEEE/CVF conference on computer vision and pattern recognition*, pages 15750–15758, 2021. 6
- [11] Xinlei Chen, Haoqi Fan, Ross Girshick, and Kaiming He. Improved baselines with momentum contrastive learning. *arXiv preprint arXiv:2003.04297*, 2020. 2
- [12] Xinlei Chen*, Saining Xie*, and Kaiming He. An empirical study of training self-supervised vision transformers. *arXiv preprint arXiv:2104.02057*, 2021. 2
- [13] Yubei Chen, Dylan Paiton, and Bruno Olshausen. The sparse manifold transform. *Advances in neural information processing systems*, 31, 2018. 2
- [14] Yubei Chen, Adrien Bardes, Zengyi Li, and Yann LeCun.

- Bag of image patch embedding behind the success of self-supervised learning. *arXiv preprint arXiv:2206.08954*, 2022. 4
- [15] Kenneth Ward Church. Word2vec. *Natural Language Engineering*, 23(1):155–162, 2017. 3
- [16] Rumen Dangovski, Li Jing, Charlotte Loh, Seungwook Han, Akash Srivastava, Brian Cheung, Pulkit Agrawal, and Marin Soljačić. Equivariant contrastive learning. *arXiv preprint arXiv:2111.00899*, 2021. 2, 3, 6
- [17] Alexandre Devillers and Mathieu Lefort. Equimod: An equivariance module to improve self-supervised learning. *arXiv preprint arXiv:2211.01244*, 2022. 2
- [18] Aleksandr Ermolov, Aliaksandr Siarohin, Enver Sangineto, and Nicu Sebe. Whitening for self-supervised representation learning. In *International Conference on Machine Learning*, pages 3015–3024. PMLR, 2021. 2
- [19] Luca Falorsi, Pim De Haan, Tim R Davidson, Nicola De Cao, Maurice Weiler, Patrick Forré, and Taco S Cohen. Explorations in homeomorphic variational auto-encoding. *arXiv preprint arXiv:1807.04689*, 2018. 2
- [20] Peter Földiák. Learning invariance from transformation sequences. *Neural computation*, 3(2):194–200, 1991. 2
- [21] Quentin Garrido, Laurent Najman, and Yann Lecun. Self-supervised learning of split invariant equivariant representations. *arXiv preprint arXiv:2302.10283*, 2023. 1, 2, 3, 4, 6, 12
- [22] Spyros Gidaris, Praveer Singh, and Nikos Komodakis. Un-supervised representation learning by predicting image rotations. *arXiv preprint arXiv:1803.07728*, 2018. 2
- [23] Ross Goroshin, Michael F Mathieu, and Yann LeCun. Learning to linearize under uncertainty. *Advances in neural information processing systems*, 28, 2015. 2
- [24] Jean-Bastien Grill, Florian Strub, Florent Altché, Corentin Tallec, Pierre Richemond, Elena Buchatskaya, Carl Doersch, Bernardo Avila Pires, Zhaohan Guo, Mohammad Gheshlaghi Azar, et al. Bootstrap your own latent—a new approach to self-supervised learning. *Advances in neural information processing systems*, 33:21271–21284, 2020. 2
- [25] Doug P Hardin, TJ Michaels, and Edward B Saff. A comparison of popular point configurations on S^2 . *arXiv preprint arXiv:1607.04590*, 2016. 4
- [26] Kaiming He, Xiangyu Zhang, Shaoqing Ren, and Jian Sun. Deep residual learning for image recognition. In *Proceedings of the IEEE conference on computer vision and pattern recognition*, pages 770–778, 2016. 6, 7
- [27] Kaiming He, Haoqi Fan, Yuxin Wu, Saining Xie, and Ross Girshick. Momentum contrast for unsupervised visual representation learning. In *Proceedings of the IEEE/CVF conference on computer vision and pattern recognition*, pages 9729–9738, 2020. 2, 5
- [28] Geoffrey E Hinton, Alex Krizhevsky, and Sida D Wang. Transforming auto-encoders. In *Artificial Neural Networks and Machine Learning—ICANN 2011: 21st International Conference on Artificial Neural Networks, Espoo, Finland, June 14–17, 2011, Proceedings, Part I 21*, pages 44–51. Springer, 2011. 2
- [29] Shun Iwase, Xingyu Liu, Rawal Khirodkar, Rio Yokota, and Kris M Kitani. Repose: Fast 6d object pose refinement via deep texture rendering. In *Proceedings of the IEEE/CVF International Conference on Computer Vision*, pages 3303–3312, 2021. 2
- [30] Wadim Kehl, Fabian Manhardt, Federico Tombari, Slobodan Ilic, and Nassir Navab. Ssd-6d: Making rgb-based 3d detection and 6d pose estimation great again. In *Proceedings of the IEEE international conference on computer vision*, pages 1521–1529, 2017.
- [31] Alex Kendall, Matthew Grimes, and Roberto Cipolla. PoseNet: A convolutional network for real-time 6-dof camera relocalization. In *Proceedings of the IEEE international conference on computer vision*, pages 2938–2946, 2015. 2
- [32] Hankook Lee, Kibok Lee, Kimin Lee, Honglak Lee, and Jinwoo Shin. Improving transferability of representations via augmentation-aware self-supervision. *Advances in Neural Information Processing Systems*, 34:17710–17722, 2021. 1, 2, 6
- [33] Amy Lin, Jason Y Zhang, Deva Ramanan, and Shubham Tulsiani. Relpose++: Recovering 6d poses from sparse-view observations. *arXiv preprint arXiv:2305.04926*, 2023. 2, 3
- [34] Aaron van den Oord, Yazhe Li, and Oriol Vinyals. Representation learning with contrastive predictive coding. *arXiv preprint arXiv:1807.03748*, 2018. 2
- [35] Maxime Oquab, Timothée Darcet, Théo Moutakanni, Huy Vo, Marc Szafraniec, Vasil Khalidov, Pierre Fernandez, Daniel Haziza, Francisco Massa, Alaaeldin El-Nouby, et al. Dinov2: Learning robust visual features without supervision. *arXiv preprint arXiv:2304.07193*, 2023. 2
- [36] Jung Yeon Park, Ondrej Biza, Linfeng Zhao, Jan Willem van de Meent, and Robin Walters. Learning symmetric embeddings for equivariant world models. *arXiv preprint arXiv:2204.11371*, 2022. 2
- [37] Nikhila Ravi, Jeremy Reizenstein, David Novotny, Taylor Gordon, Wan-Yen Lo, Justin Johnson, and Georgia Gkioxari. Accelerating 3d deep learning with pytorch3d. *arXiv:2007.08501*, 2020. 4
- [38] Franz Scherr, Qinghai Guo, and Timoleon Moraitis. Self-supervised learning through efference copies. *Advances in Neural Information Processing Systems*, 35:4543–4557, 2022. 2
- [39] Mehran Shakerinava, Arnab Kumar Mondal, and Siamak Ravanbakhsh. Structuring representations using group invariants. *Advances in Neural Information Processing Systems*, 35:34162–34174, 2022. 2
- [40] Brian Shaler, Dan Gill, Maggie, Mark McDonald, Patricia, and Will Cukierski. Carvana image masking challenge. <https://kaggle.com/competitions/carvana-image-masking-challenge>, 2017. 2, 6, 7
- [41] Ken Shoemake. Animating rotation with quaternion curves. In *Proceedings of the 12th annual conference on Computer graphics and interactive techniques*, pages 245–254, 1985. 6
- [42] Weiwei Sun, Andrea Tagliasacchi, Boyang Deng, Sara Sabour, Soroosh Yazdani, Geoffrey E Hinton, and Kwang Moo Yi. Canonical capsules: Self-supervised capsules in canonical pose. *Advances in neural information processing systems*, 34:24993–25005, 2021. 2

- [43] Robin Winter, Marco Bertolini, Tuan Le, Frank Noé, and Djork-Arné Clevert. Unsupervised learning of group invariant and equivariant representations. *Advances in Neural Information Processing Systems*, 35:31942–31956, 2022. 2
- [44] Laurenz Wiskott and Terrence J Sejnowski. Slow feature analysis: Unsupervised learning of invariances. *Neural computation*, 14(4):715–770, 2002. 2
- [45] Zhirong Wu, Yuanjun Xiong, Stella X Yu, and Dahua Lin. Unsupervised feature learning via non-parametric instance discrimination. In *Proceedings of the IEEE conference on computer vision and pattern recognition*, pages 3733–3742, 2018. 1, 6
- [46] Yuyang Xie, Jianhong Wen, Kin Wai Lau, Yasar Abbas Ur Rehman, and Jiajun Shen. What should be equivariant in self-supervised learning. In *Proceedings of the IEEE/CVF Conference on Computer Vision and Pattern Recognition*, pages 4111–4120, 2022. 2
- [47] Yang You, Igor Gitman, and Boris Ginsburg. Large batch training of convolutional networks. *arXiv preprint arXiv:1708.03888*, 2017. 6
- [48] Jason Y Zhang, Deva Ramanan, and Shubham Tulsiani. Rel-pose: Predicting probabilistic relative rotation for single objects in the wild. In *European Conference on Computer Vision*, pages 592–611. Springer, 2022. 2, 3
- [49] Roland S Zimmermann, Yash Sharma, Steffen Schneider, Matthias Bethge, and Wieland Brendel. Contrastive learning inverts the data generating process. In *International Conference on Machine Learning*, pages 12979–12990. PMLR, 2021. 3, 12

Trajectory Regularization Enhances Self-Supervised Geometric Representation

Supplementary Material

In this supplementary material, we provide details omitted in the main text including:

- Section **A**: Comparison with similar datasets proposed in related work;
- Section **B**: Additional ablation study on the trajectory loss and the backbone architecture;
- Section **C**: Details of the mid-layer representation compression;
- Section **D**: Empirical study on the similarity between mid-layer features and patch embedding.

A. Dataset Comparison

Our benchmark proposes a dataset generation/rendering configuration that **1**) adheres to the self-supervised learning (SSL) setting where neither semantic nor geometric labels are used for training; **2**) allows evaluation on out-of-domain data with the introduction of the relative pose. We demonstrate the configuration on the ShapeNet dataset [6] as an example. There exist similar datasets derived from ShapeNet, such as 3DIEBench [21] and 3DIdent [49]. Although such datasets are designed for or suitable for benchmarking SSL geometric representations, we still provide comparisons in Table 6 given they are also derived from ShapeNet.

Table 6. Comparison with other datasets consisting of rendered images of objects from ShapeNet [6]. Our dataset **1**) does not use pose labels for training and adheres to SSL geometric representation evaluation setting; **2**) enables evaluation on out-of-domain data; **2**) has complete and even pose coverage for rendered images.

	Our dataset	3DIEBench	3DIdent
Out-of-domain evaluation	Yes	No	No
Pose coverage	$(-\pi, \pi)$	$(-\pi/2, \pi/2)$	$(-\pi/2, \pi/2)$
Pose sampling method	even	uneven	uneven
Numer of images	1.5M	2.5M	275k

B. Additional Ablation Study

Non-Equidistant Poses. Our method works when the adjacent views in the trajectory loss are sampled from smooth trajectories, where the speed varies gradually. We show this with an empirical experiment in Table 7. Adjacent views exhibit non-equidistant poses during training: we randomly sample cubic Bézier curves with the starting pose p_L and ending pose p_R , where the angle between p_L, p_R is $(5^\circ, 20^\circ)$. The middle pose p_C is randomly sampled from the curve to simulate the speed variation. Non-equidistant pose trajectory regularization also gives 4% gain.

Different Backbones. We study if the performance gain of mid-layer representations generalizes to other network/backbone architectures. For VICReg [2] with trajec-

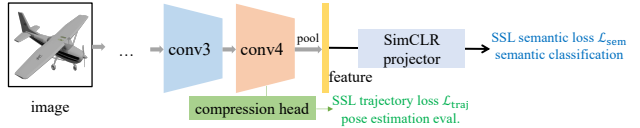


Figure 11. We compress mid-layer representation from “conv4” layer, taking SimCLR [8] as an example. For the semantic loss, we follow SimCLR’s setting and add the loss after SimCLR projector. For the pose loss, we use an MLP-based head to compress mid-layer features and the compressed feature to classify pose. Trajectory loss is put after the compression head.

tory loss, on ResNet50 backbone we also observe a similar trend of improvement with mid-level features as the ResNet18 backbone (Table 8).

C. Compression Layer

For clarity, we provide details on compressing mid-layer representations of SimCLR [8] (Fig.11). For the semantic loss and downstream semantic classification, we always follow the baseline setting and make no changes. We take SimCLR as an example. For pose estimation, we use an MLP-based head to compress mid-layer features and the compressed feature to classify pose. Trajectory is also put post-compression-head.

D. Mid-Layer Features and Patch Embedding

As mentioned earlier, the improved SSL geometric representation quality by mid-layer representations could be partly attributed to the similarity to the patch embedding. Empirically, for the VICReg [2] baseline, we partition the

Table 7. We render adjacent views that exhibit non-equidistant poses. Similar to equidistant poses, the trajectory loss with non-equidistant poses also gives 4% gain for relative pose estimation.

	Rel. pose acc(%)
VICReg	76.7
VICReg+equidistant traj.	80.5
VICReg+non-equidistant traj.	80.3

Table 8. For VICReg [2] with the proposed trajectory loss, we use different backbones and also observe performance gains of relative pose estimation accuracy with mid-layer representations.

Rel. pose acc(%)	feature	conv4	conv3
Res18	80.5	88.3	89.4
Res50	82.6	90.1	91.0

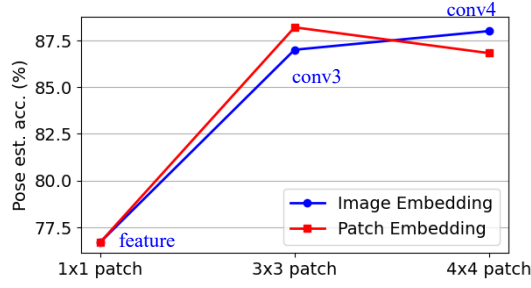


Figure 12. Mid-layer representations improve SSL geometric representation quality, which could be partly attributed to the similarity to the patch embedding. Empirically, a similar trend of pose estimation accuracy gain was observed with patch embedding. The metric is relative pose estimation accuracy on in-domain data.

input image to $m \times m$ patches ($m = 1, 3, 4$ in our experiment). As in Fig. 12, using patch embedding has a similar effect as mid-layer representation and also improves the pose estimation accuracy.